ANNUAL REPORT

Detecting Small-Scale Topographic Changes and Relict Geomorphic Features on Barrier Islands Using SAR

Year 2

James C. Gibeaut*, Melba M. Crawford**, Roberto Gutierrez*, K. Clint Slatton**, Amy L. Neuenschwander**, and Michael R. Ricard**

Prepared for the National Atmospheric and Space Administration (NASA)
Office of Mission to Planet Earth
Topography and Surface Change Program

NASA Grant No. NAG 5-2954

*Bureau of Economic Geology
Noel Tyler, Director
The University of Texas at Austin
Austin, Texas 78713-8924

**Center for Space Research
The University of Texas at Austin
Austin, Texas 78759-5321

July 1997

ANNUAL REPORT

Detecting Small-Scale Topographic Changes and Relict Geomorphic Features on Barrier Islands Using SAR

Year 2

James C. Gibeaut*, Melba M. Crawford**, Roberto Gutierrez*, K. Clint Slatton**, Amy L. Neuenschwander**, and Michael R. Ricard**

Prepared for the National Atmospheric and Space Administration (NASA)
Office of Mission to Planet Earth
Topography and Surface Change Program

NASA Grant No. NAG 5-2954

*Bureau of Economic Geology
Noel Tyler, Director
The University of Texas at Austin
Austin, Texas 78713-8924

**Center for Space Research
The University of Texas at Austin
Austin, Texas 78759-5321

July 1997

ANNUAL REPORT

Detecting Small-Scale Topographic Changes and Relict Geomorphic Features on Barrier Islands Using SAR

Year 2

James C. Gibeaut*, Melba M. Crawford**, Roberto Gutierrez*, K. Clint Slatton**, Amy L. Neuenschwander**, and Michael R. Ricard**

Prepared for the National Atmospheric and Space Administration (NASA)
Office of Mission to Planet Earth
Topography and Surface Change Program

NASA Grant No. NAG 5-2954

*Bureau of Economic Geology
Noel Tyler, Director
The University of Texas at Austin
Austin, Texas 78713-8924

**Center for Space Research
The University of Texas at Austin
Austin, Texas 78759-5321

July 1997

Contents

Appendices (attached)

Introduction

The shapes and elevations of barrier islands may change dramatically over a short period of time during a storm. Coastal scientists and engineers, however, are currently unable to measure these changes occurring over an entire barrier island at once. This three-year project, which is funded by NASA and jointly conducted by the Bureau of Economic Geology and the Center for Space Research at The University of Texas at Austin, is designed to overcome this problem by developing the use of interferometry from airborne synthetic aperture radar (AIRSAR) to measure coastal topography and to detect storm-induced changes in topography. Surrogate measures of topography observed in multiband, fully polarimetric AIRSAR (This type of data are now referred to as POLSAR data.) are also being investigated.

Digital elevation models (DEM) of Galveston Island and Bolivar Peninsula, Texas (Fig. 1) obtained with Topographic SAR (TOPSAR) are compared with measurements by Global Positioning System (GPS) ground surveys and electronic total station surveys. In addition to topographic mapping, this project is evaluating the use of POLSAR to detect old features such as storm scarps, storm channels, former tidal inlets, and beach ridges that have been obscured by vegetation, erosion, deposition, and artificial filling. We have also expanded the work from the original proposal to include the mapping of coastal wetland vegetation and depositional environments. Methods developed during this project will provide coastal geologists with an unprecedented tool for monitoring and understanding barrier island systems. This understanding will improve overall coastal management policies and will help reduce the effects of natural and man-induced coastal hazards. This report summarizes our accomplishments during the second year of the study. Also included is a discussion of our planned activities for year 3 and a revised budget.

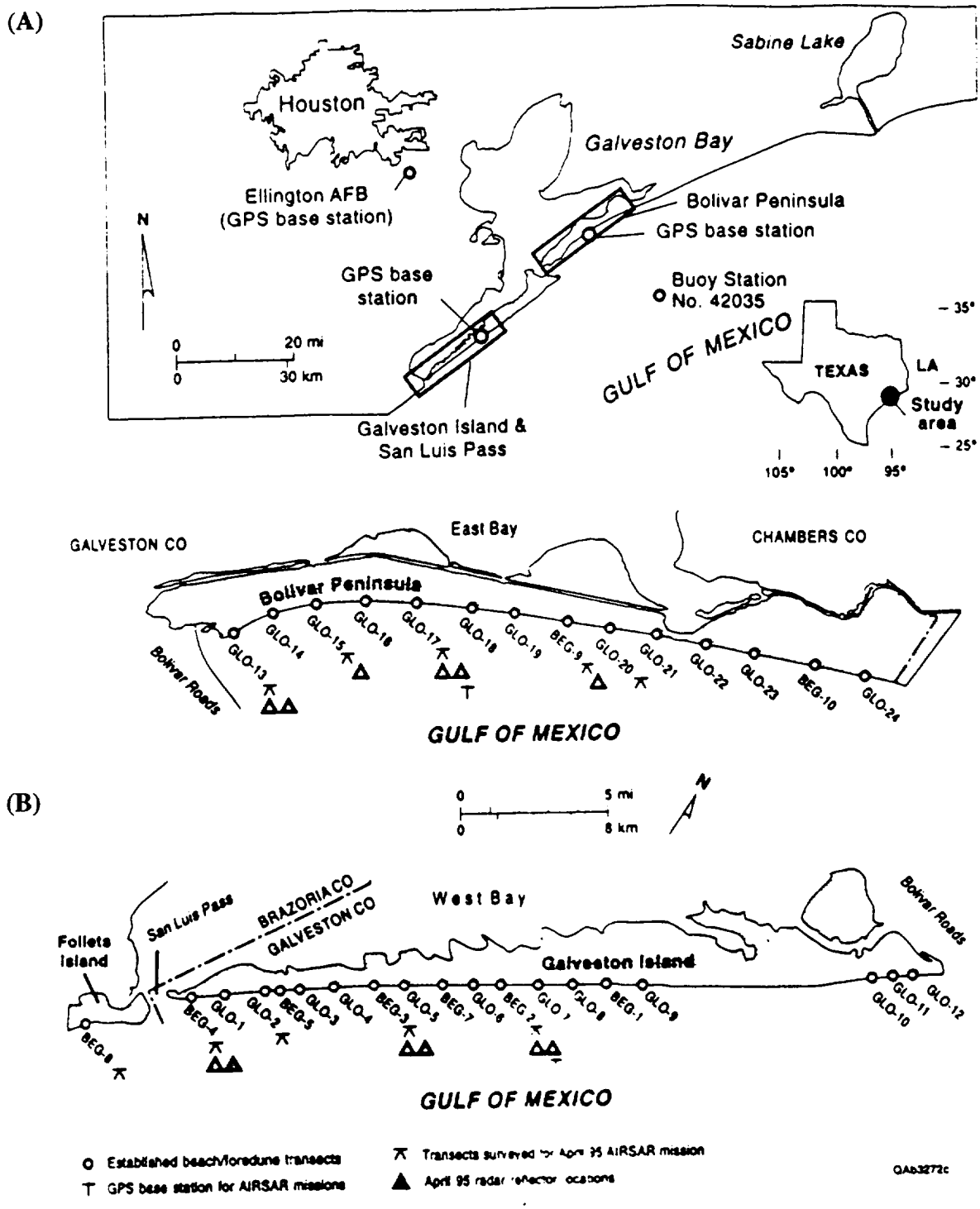

Figure 1. Study areas for 1995 and 1996, AIRSAR missions. **(A)** Locations of study areas on Galveston Island and Bolivar Peninsula. Also shown are GPS base stations operated during the flights. In 1995, the NASA DC-8 aircraft took off from Ellington Airforce Base for each flight. In 1996, the aircraft came from Dallas. Buoy Station No. 42035 is operated continuously by the National Data Buoy Center and provides wave and meteorological data. **(B)** Detail of study areas.

1996 AIRSAR Missions

We completed our 1996 AIRSAR missions in June. On June 24, we imaged along the coast from Freeport, Texas northeast to Bolivar Roads (the entrance to Galveston Bay). The Gulf of Mexico shoreline is in the center of the swath, and the coverage includes all of Follets and Galveston Islands. On June 25, we imaged from Bolivar Roads northeast to High Island, Texas again with the Gulf shoreline in the center of the swath and covering all of Bolivar Peninsula. Also on the 25th, we imaged along a line oriented perpendicular to the Gulf shoreline from Crystal Beach on Bolivar Peninsula north to Liberty, Texas north of Galveston Bay.

During both days, we operated a geodetic-quality GPS base station on the ground and one on the DC-8 aircraft (Fig. 1). Just before the flights, we placed and surveyed 16 radar reflectors (1 m sheet metal corner reflectors) along the flight lines to aid with image registration. Within 8 days of the mission, we completed detailed GPS surveys of a 2-km stretch of beach on Galveston Island and additional GPS surveys along 6 transects over the study area. These ground surveys are required to check the TOPSAR topographic solutions.

Also within a few days of the flights, we conducted detailed vegetation and sediment surveys at a test site on Bolivar Peninsula. The test site includes uplands, high and low marshes, barren high and low flats, and open water. The ground data are required for interpreting the environmental mapping capability of POLSAR data.

For the two areas imaged along the shoreline, we collected 20 MHz, C-, L-, and P-band POLSAR, 40 MHz C- and L-band POLSAR, and front (from the Gulf of Mexico side) and back looks of 40 MHz C- and L-band TOPSAR. For the shore-perpendicular area, we obtained 20 MHz, C-, L-, and P-band POLSAR and 40 MHz C- and L-band POLSAR. We have requested most of the POLSAR data and the front look of the TOPSAR data to be processed by NASA's Jet Propulsion Laboratory (JPL) and transmitted to us.

In addition to the radar data, we obtained calibrated Airborne Multispectral Scanner (CAMS) data and simultaneous color infrared photography of Galveston Island and Bolivar Peninsula on July 3, 1996. NASA's Stennis Space Flight Center acquired these

data. The CAMS data have a 4-m ground resolution which is the same as the 40 MHz SAR data.

Data

Status of the 1996 Data

(1) We have received about 90 percent of the requested 20 and 40 MHz POLSAR data. The data cover all of Bolivar Peninsula and Galveston Island and some of Follets Island southwest of Galveston Island. We also obtained several frames from the Trinity River Delta area in northern Galveston Bay. Some of our data have been affected by a calibration problem in JPL's AIRSAR processor. The C-band, horizontal/vertical dipole channel was not calibrated properly. JPL is reprocessing these data.

(2) We have received two TOPSAR frames covering 20 km of the southwest end of Bolivar Peninsula.

(3) We have all the kinematic and static GPS data and other topographic survey data taken on the ground during the missions and are acquiring the GPS data taken on the aircraft from JPL.

(4) We have vegetation, and sediment data for the test site including numerous photographs taken on the ground.

(5) We have all the CAMS data and vertical aerial photography.

(6) We have acquired National Wetlands Inventory digital data and entered them into our Geographic Information System (GIS).

Status of the 1995 Data

(1) In April, 1995, we acquired 20 MHz POLSAR and 40 MHz TOPSAR data for Galveston and Follets Islands and Bolivar Peninsula. We have obtained all of the 20-MHz, POLSAR data for one front look direction and several frames for the back look direction.

(2) We obtained two frames of TOPSAR data covering about 20 km of the southwest end of Galveston Island.

(3) We have all the kinematic GPS data taken on the ground during the missions and are acquiring the data taken on the aircraft from NASA.

(4) We have acquired and reduced all ground survey data taken by us during the missions, and we have transmitted the X,Y,Z positions of the radar reflectors for the Galveston area to JPL. In addition to the topographic data we collected, we have obtained topographic transect data of Bolivar Peninsula taken by a commercial surveyor in 1992.

(5) We have acquired digital data of roads and hydrography and have entered the data into our GIS.

(6) We acquired one high-quality vertical aerial photograph of Bolivar Peninsula taken at 1:40,000 scale by the U.S. Geological Survey.

Data Analysis

We have reduced and compiled all topographic survey data acquired by us on the ground during the missions. We have used these data to georeference radar images and to make a preliminary evaluation of the TOPSAR DEM on the southwest end of Bolivar Peninsula. We conducted preliminary work on techniques to filter noise, mosaic, and georeference TOPSAR DEM's from low-relief (<10 m) coastal areas. We finished development of a radar backscatter simulation model and have incorporated into it vegetation and sediment observations from the Bolivar Peninsula test site. This model provides information on the relative importance of microwave scattering from the surface and vegetation in various coastal wetland environments. We have begun to use the POLSAR and CAMS data to classify coastal wetland environments on Bolivar Peninsula. We are continuing development of our own software for repeat-pass interferometry.

Preliminary Results

We prepared abstracts and proceedings papers describing our work on this project over the last year. Two manuscripts have been submitted for publication in the 1997 International Geoscience and Remote Sensing Symposium Proceedings. One describes our work with evaluating, mosaicing, georeferencing, and improving TOPSAR DEM's

from low-relief regions (see Appendix A). The other paper addresses multisensor classification of coastal wetlands using POLSAR and CAMS data (see Appendix B). We also presented a poster at the Fourth International Conference on Remote Sensing for Marine and Coastal Environments (see Appendix C). This poster won an "honorable mention" award. Clint Slatton completed a Master of Science in Engineering Thesis (see Appendix D). His thesis involved the development and testing of a model that simulates radar backscatter from coastal wetland environments. The following is a summary of our results.

The study areas on Galveston Island and Bolivar Peninsula have a relief of less than 4 m and are composed of distinct subenvironments and morphological features. These subenvironments and features include multiple beach ridges and swales, vegetated barrier flats, foredunes, high- and low-salt-water marshes, intertidal/wind-tidal flats, tidal creeks, tidal deltas, and exposed and sheltered beaches. Also present are relict washover fan/flood-tidal delta complexes. Salinity, vegetation, sediment/soil type, and surface roughness vary significantly between these areas. Beach ridges have dry, shelly sand sediment, and intervening swales between ridges are wetter with some having standing water. Barrier flats are also made of shelly sand and support land uses such as agriculture, ranching, and urban/recreational development. Sediments forming salt-water marshes and intertidal/wind-tidal flats contain more mud, are wetter, and potentially have a higher salinity than other environments. Sediments on active ocean-side beaches are fine sand with a large alongshore variation in gravel-sized shell content. Foredunes behind the beaches consist of dry well-sorted sand.

During the first year of this project we demonstrated that multiband POLSAR data are able to separate various subenvinronments and morphological features very well. In general, we found that C-band is well suited for detailed vegetation discrimination, whereas L- and P-band are better for separating the imagery into larger scale environmental units based on both vegetation and substrate characteristics. Furthermore, L-band appears to best delineate beach ridge and swale morphology. L- and P-band data appear to indicate extensions of tidal creeks cutting across the islands that may not be

visible on aerial photography. L- and P-band can also delineate former breaches caused by storms and dredging.

During the past year, we began to apply statistical classification techniques to the 4-m resolution(40 MHz) C- and L-band POLSAR data and CAMS data. The goal of this work is to develop land cover maps with classifications that are geologically and biologically significant. Data were classified on a single-sensor and multisensor basis. The most reliable single-sensor classification was obtained using CAMS optical data. POLSAR data were second in classification accuracy and CAMS thermal data last. When multisensor integration was performed using the single-sensor classifiers, classification accuracy increased. This indicates that POLSAR data contain useful information in delineating coastal wetlands (see Appendix B for more details).

Evaluation and processing of TOPSAR DEM's obtained during the last year has provided some promising results. Because the study area has low relief, noise or systematic error with a magnitude as small as 0.5 m is apparent and significantly limits the DEM's use. It was readily obvious that the 1995 TOPSAR DEM of the southwest end of Galveston Island was not useful. Systematic and apparently random errors on the order of the relief of the island were present. The 1995 data were taken in non-pingpong mode (transmit off the top antenna only) whereas the 1996 data were obtained in pingpong mode (alternating the transmit antenna between the top and bottom antennas). Pingpong mode effectively doubles the antenna baseline which improves the root mean square height error by a factor of two (Yunling Lou (JPL), e-mail communication, June 30, 1997).

The 1996 DEM of the southwest end of Bolivar Peninsula shows much improvement over the 1995 data from Galveston Island. Figure 2 is one frame of the DEM obtained with C-band, 40 MHz TOPSAR with radar illumination from the Gulf of Mexico side (our front look). The azimuth direction (flight path direction) is roughly parallel to the peninsula (horizontal direction in figure 2). The radar incidence angle was 45 degrees along the axis of the peninsula. Maximum relief of this region is about 6 m. The shading interval in figure 2 is 9 cm and the pixels are 10 m by 10 m.

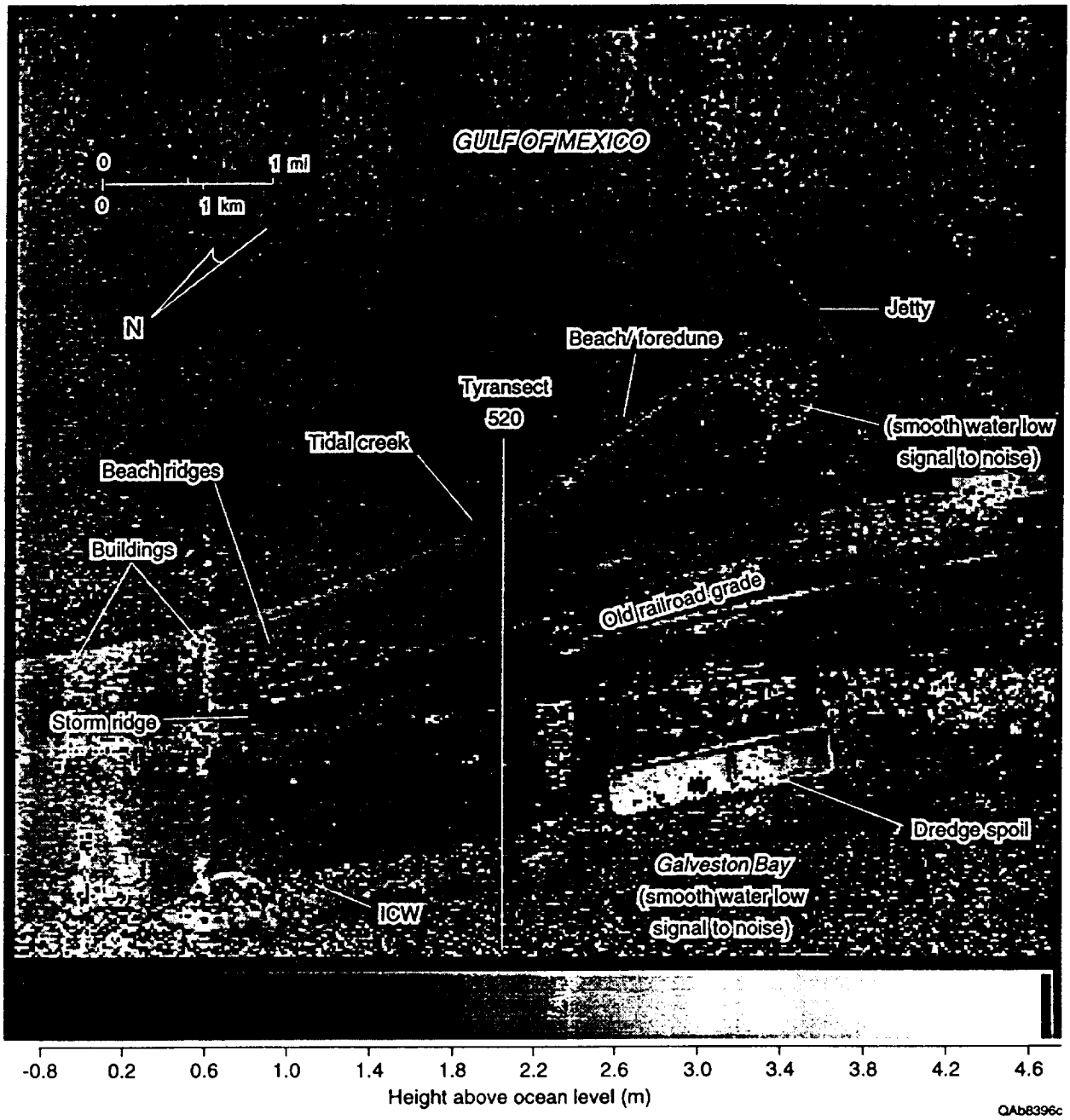

Figure 2. TOPSAR DEM from the southwest end of Bolivar Peninsula. Ground pixel size is 10 m by 10 m.

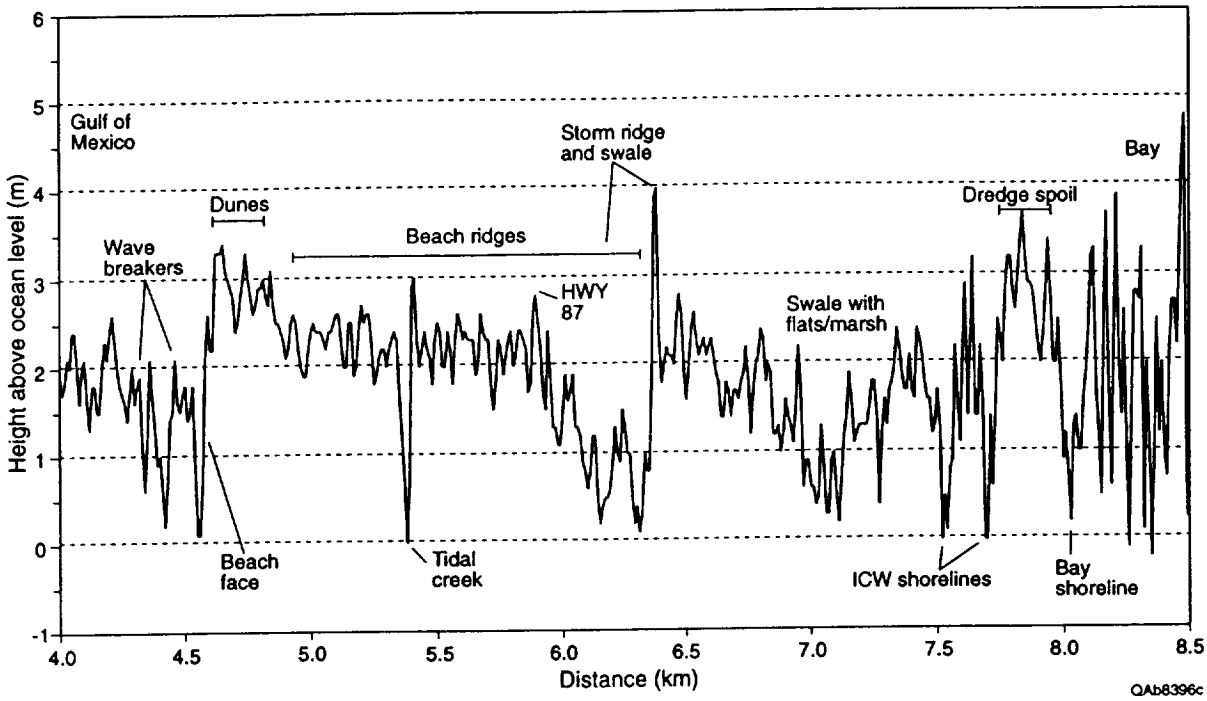

Figure 3. Topographic transect #520 extracted from the DEM in figure 2.

Topographically subtle features such as the beachface, foredune, beach ridges and swales, and an old railroad grade are apparent (figure 2). There are, however, vertical bands especially pronounced in the near range (top of figure 2). The DEM, as received from JPL, had more prominent banding than what is shown here. We processed the data to remove as much of the banding over land as possible. This systematic error is caused by aircraft motion and, before our processing, had an amplitude that varied in range (top to bottom direction in figure 2) from 1 to 5 m. Our processing involved extracting a strip of data from over the Gulf of Mexico and parallel to the azimuth direction. This strip was 160 pixels wide in the range direction. The pixels were averaged across range to yield a curve that was added to the rest of the DEM up and down range. This correction curve was subsequently adjusted by a constant factor to obtain the best looking DEM over the land areas. This technique significantly improved the DEM, but it only worked because the Gulf of Mexico is a relatively flat surface and extends across the entire azimuth direction of the frame. Also important to the success of this approach is that the banding is oriented parallel to the range direction. We have also attempted harmonic filtering techniques, but so far this has not satisfactorily improved the DEM.

Figure 3 is a transect taken from the DEM in figure 2. This transect crosses the zone where waves are breaking, the beach, dune, beach ridges, tidal creek, and the intracoastal waterway (ICW). Areas where there is a smooth surface, such as in the bays and ICW, radar backscatter is low. In these areas, therefore, the signal to noise ratio for the TOPSAR is low and the heights noisy. The transect shows the ocean height at the beach face, the height of the tidal creek, the heights of the ICW shorelines, and the height of the bay shoreline all to be within 20 cm, which is expected. This result indicates the internal consistency of the DEM. At this point in our analysis, we think TOPSAR DEM's are useful for aiding the classification of subenvironments in low-relief coastal areas and may be useful in measuring large-scale erosion caused by hurricanes.

Plans for Year 3

(1) At this time, we are not certain of the timing of our third AIRSAR mission. We are, however, moving forward with plans for a laser altimeter mission.

(2) We will continue to work with JPL in evaluating TOPSAR DEM's using data from Bolivar Peninsula. We will evaluate the accuracy and resolution of the TOPSAR DEM with ground surveys and laser altimeter data if available.

(3) We will continue to use physically based scatterer models to analyze the SAR interactions with wetland terrain and vegetation. We will continue to assess SAR's sensitivity to parameters that are important for the ecological study of wetland ecosystems, such as soil moisture, soil salinity, soil type, and vegetation cover.

(4) We will continue work on applying POLSAR to classify barrier island environments and geomorphic features and to produce maps of select areas. We will also continue work on incorporating POLSAR into multisensor classification schemes. A significant step will be the addition of TOPSAR DEM's to the classification process.

Budget Summary

(Date) From 9/1/97 to 8/31/98

		NASA USE ONLY	
	A	B	C
1. Direct Labor (salaries, wages, and fringe benefits)	$ 41,919		
2. Other Direct Costs:			
a. Subcontracts	$ 0		
b. Consultants	$ 0		
c. Equipment	$ 0		
d. Supplies	$ 1,500		
e. Travel	$ 6,420		
f. Other	$ 7,500		
3. Indirect Costs	$ 27,420		
4. Other Applicable Costs			
5. Subtotal-Estimated Costs	$ 84,759		
6. Less Proposed Cost Sharing (if any)	$ 0		
7. Carryover Funds (if any)			
a. Anticipated amount $5,000			
b. Amount used to reduce budget	$ 84,759		
8. Total Estimated Costs			XXXXXXXX
APPROVED BUDGET	XXXXXXXX	XXXXXXXX	

Instructions

1. Provide a separate budget summary sheet for each year of the proposed research.
2. Grantee estimated costs should be entered in Column A. Columns B and C are for NASA use only. Column C represents the approved grant budget.
3. Provide in attachments to the budget summary the detailed computations of estimates in each costs category, along with any narrative explanation required to fully explain proposed costs.

----------ADDITIONAL INSTRUCTIONS ON REVERSE----------

Appendix A

Manuscript submitted to the 1997 International Geoscience and Remote Sensing Symposium to be held August 4 to 8 in Singapore.

Removal of Residual Errors From SAR-Derived Digital Elevation Models For Improved Topographic Mapping of Low-Relief Areas

K. Clint Slatton[1], Melba M. Crawford[1], James C. Gibeaut[2], and Roberto Gutierrez[2]
(1): Center for Space Research, University of Texas at Austin
3925 W. Braker Ln., Suite 200, Austin, TX 78759-5321
(2): Bureau of Economic Geology, University of Texas at Austin
E-mail: slatton@csr.utexas.edu; Ph: (512) 471-5509; Fax: (512) 471-3570

Abstract -- Interferometric synthetic aperture radar data can be used to precisely map topography, but low-relief areas are problematic because errors in the data can be large compared to the topographic variations. The NASA/JPL TOPSAR system acquired data over a low-relief test site on the Texas coast in 1996. Due to unusually high turbulence during the acquisition and the mild topography, residual height errors were visible in the Digital Elevation Model (DEM). The characteristics of the error signal are described and a method is outlined for removing the residual error and mosaicking the affected TOPSAR frames.

INTRODUCTION

Land surfaces with mild topography, such as river floodplains and coastal zones, are typically very prone to flooding due to precipitation and storm-surge events. Topography-based flood models have been developed that predict the extent and severity of flooding in such areas under a variety of circumstances, and Digital Elevation Models (DEMs) are needed as inputs to these topography-based models [1]. Because errors in the DEMs propagate directly into the predictions of flood extent, it is important to maximize the accuracy and precision of the DEMs that are used in these models.

Standardized and georeferenced DEMs are produced by the United States Geological Survey (USGS) and are widely available for most of the United States. These DEMs are often sufficiently precise for areas with significant topography because any height errors will typically be small relative to the actual surface height variations. The specification for the Level 1 USGS DEM is ≤15 m vertical root mean square (rms) error. Figure 1 shows a Level 1 DEM for the test site. The horizontal data spacing is 30 m and the vertical data spacing is 1 ft [2]. However, greater precision is needed when mapping low-relief areas because these errors in the DEMs may be of similar magnitude to the surface height variations, and so have a great effect on the accuracy of flood models that use the DEMs. DEMs used for flood modeling must also have fine horizontal resolution so that small hydrologically-important features, such as stream beds, are accurately mapped. Improved resolution can potentially be achieved by generating DEMs using radar data.

In June 1996, the NASA/JPL AIRSAR system collected interferometric synthetic aperture radar (INSAR) data over low-relief regions on the coast of Texas, USA. To collect INSAR data, the AIRSAR system operates in its topographic (TOPSAR) mode. Figure 2 shows two mosaicked TOPSAR frames over Mission Bay, Texas. The ground-range-projected TOPSAR DEMs have data spacings of 10 m horizontally and 0.1 m vertically. The TOPSAR data are within sensor specifications in terms of rms height error [3]. However, small systematic height errors are still visible in the original DEMs because the area has such low relief. This paper describes some of the errors observed in the data and outlines the procedures used to minimize those errors and mosaic the DEMs.

INSAR BACKGROUND

DEMs, like those produced by the USGS, have traditionally been derived from stereo processing of aerial photography or optical spaceborne data. In recent years, DEMs have also been derived from SAR data using interferometric processing. The data for INSAR DEMs may be acquired day or night and in most weather conditions, but the primary advantage of INSAR methods is that the elevation of each pixel is determined independently. In stereo-optical DEMs, individual pixels are binned into discrete elevations to create noise-free closed-contour topographic maps. The primary disadvantages of INSAR DEMs are their sensitivity to sensor motion and their noise characteristics.

DEMs can be generated from INSAR data by combining two complex (phase and magnitude) SAR images acquired from similar vantage points [4]. Once the two images are co-registered, a differential phase can be calculated for each pixel. Using a known position of at least one pixel and unwrapping the modulo 2π phase, a map of absolute phase differences is generated. Geometric relationships can then be used to create a height map (DEM) relative to the radar position. The height map can be referenced to a geocentric coordinate system by collecting Global Positioning System (GPS) data onboard the sensor platform.

Most of the work to date in generating INSAR DEMs has focused on data collected from spaceborne systems using multiple observations (repeat-pass). In particular, the European Remote Sensing satellites (ERS-1 and -2) have been used extensively for this purpose [5]. However, any

This work was supported by the Texas Regional Change Program through the Texas Space Grant Consortium and the Johnson Space Center, a National Aeronautics and Space Administration grant under the Topography and Surface Change Program (Grant NAG5-2954), and the Texas Advanced Technology Program.

changes that occur in surface or atmospheric conditions in the imaged area between observations will introduce errors into the subsequent DEM. The shortest time interval between observations suitable for INSAR processing is about one day for the tandem ERS system [6]. Significant changes in the backscattering properties of the surface or refractive properties of the atmosphere due to precipitation or humidity changes can occur on this time scale, thus reducing the number of suitable image pairs [7].

INSAR systems with more than one antenna, such as TOPSAR, can make dual observations simultaneously so that decorrelation of the scene through time is not a factor. This is especially important for vegetated, humid regions, such as the Texas coast, which can decorrelate rapidly. TOPSAR data are also available at higher spatial resolution than currently-available spaceborne data, (e.g. 25 m for ERS-1). This improves the mapping of small-scale features. The primary disadvantage of single-pass airborne systems is that the platform motion is perturbed more frequently and in a less deterministic manner than spaceborne platforms. Standard processing of TOPSAR data does include motion compensation, but if the motion is severe or high-frequency, residual errors on the order of $\pm$ 1.5 m may be observed in the DEMs. If the actual topographic variations are on the order of $\leq$10 times this magnitude, the error signal may be visible in the DEMs.

TEST SITE

TOPSAR flightlines were acquired along coastal stream beds in the San Antonio-Nueces watershed on the Texas coast. This watershed is located on a low-lying coastal plain. Flightlines were oriented approximately normal to the shoreline to observe the topography along the streams that carry most of the water runoff to the bays. The topographic variation in the 20 km nearest to the shore is only about 13 m. The TOPSAR data analyzed for this paper are from a flightline over Mission Bay. Hurricane models implemented for similar areas along the Texas coast predict storm surge penetrations of up to 15 km inland for a category 1 hurricane (74-95 mph winds), with flooding distributions that are highly dependent upon small topographic variations such as stream beds [1].

CHARACTERIZING THE DATA

1st order errors in the TOPSAR DEMs are manifest as planar tilting in range. This tilting is the result of uncompensated path delays in the radar system. When mapped into heights, those time delays can produce linear slopes in the DEMs. The DEMs can also exhibit higher order errors due to aircraft motion. Errors due to aircraft motion were observed in one of the TOPSAR frames over the Mission Bay test site.

Two adjacent 10 km x 10 km TOPSAR frames were acquired from a single flightline. A periodic signal superimposed on the topography was apparent in one of the frames. This "ripple" was primarily a function of azimuth, but also exhibited a weak inverse dependence on range. The approximate peak-to-peak amplitude was 3 m, and there were 8 complete periods in the frame. A printout of the aircraft motion file was obtained and the ripple signal appeared to be exactly correlated with the roll motion of the aircraft, which exhibited an 8 Hz frequency and peak-to-peak amplitude of 1°. Neither yaw nor pitch motion exhibited any significant correlation with the ripple signal.

TOPSAR DEMs have demonstrated relative rms height errors of 1-2 m in relatively flat areas [3]. The DEMs acquired over this test site exhibited rms error levels well within those reported levels. The residual errors due to aircraft motion were visible because nearby storms produced excessive turbulence during the acquisition and the total topographic variation in the test site is only about 10 times the magnitude of the residual signal.

ERROR REMOVAL AND EVALUATION

To produce a mosaicked DEM strip from individual TOPSAR frames, the relative errors must be corrected. After an internally consistent DEM strip is produced, it can be georeferenced using GPS data collected on the ground. The following procedures were followed.

1.0 Correct relative errors
- 1.1 filter out the motion signal
- 1.2 image-to-image registration
  - 1.2.1 1st order correction of elevations
  - 1.2.2 standard 2-dimensional registration
- 1.3 smooth noise over low-backscatter targets

2.0 Georeference the DEM strip
- 2.1 image-to-GPS registration
  - 2.1.1 1st order correction of elevations
  - 2.1.2 standard 2-dimensional registration

It is necessary to correct the relative errors before georeferencing so that overlapping portions of adjacent DEMs will only differ to a 1st order. A stop-band Infinite Impulse Response (IIR) filter was used to remove the ripple signal. The filter removed the 8 Hz ripple while preserving small-scale topographic features.

Elevations of features in the overlap between the two DEMs were used to add the best planar correction (in a least squares sense) to the slave DEM to obtain agreement with the master DEM's elevations to a 1st order. Those same control points were then used to do a 2-dimensional image-to-image registration to mosaic the two DEMs. JPL is currently developing the capability to output continuous strips of TOPSAR data, which will eliminate the need for mosaicking frames on a single flightline. Some open water areas in the far range of the DEMs exhibited very low signal to noise ratios (SNR), which were manifest as regions with very high-frequency, large-magnitude noise. These areas were assigned a constant elevation equal to elevation of the surrounding bank.

Georeferencing the DEMs was accomplished via 3-dimensional registration to GPS tie points after the DEMs were made internally consistent and mosaicked. The DEMs are georeferenced during the operational processing at JPL by giving the latitude/longitude of the scene center, but more accurate *in situ* georeferencing is needed for the DEMs in low-relief areas.

Static GPS points were collected for georeferencing, but more static GPS points will be collected to validate these results. Kinematic GPS transects have also been collected along several roads in the imagery, but the solutions have not yet been analyzed. Figure 3 shows transects extracted from the co-registered TOPSAR and USGS DEMs. The transects show that the superior resolution of TOPSAR allows it to capture topographic variations that are not resolved in the USGS DEM. The TOPSAR data also exhibit greater variability due to noise and non-surface features such as trees.

CONCLUSIONS

The higher-order errors observed in these data do not appear to be significant in most TOPSAR DEMs. The errors were visible in these data because of the extreme low-relief of the region and the proximity of storms during the acquisition.

Future work will include improvements to the filtering of the motion signals and validation of the results with more GPS surveys. However, these preliminary results do indicate that systematic errors can be minimized and precise DEMs can be generated for low-relief areas using TOPSAR data.

REFERENCES

[1] Texas A&M University, College of Architecture, Storm Atlas: Brazoria, Galveston, and Harris Counties, Texas A&M University, pg. 3-1, September 1993.

[2] United States Geologic Survey (USGS), Digital Elevation Models: Data Users Guide 5, USGS, pg. 14, 1993.

[3] Madsen, S. N., J. M. Martin, and H. A. Zebker, "Analysis and Evaluation of the NASA/JPL TOPSAR Across-Track Interferometric SAR System", *IEEE Trans. Geosci. Remote Sensing*, vol. 33, no. 2, pg. 383-391, March, 1995.

[4] Zebker, H. A. and R. M. Goldstein, "Topographic Mapping from Interferometric Synthetic Aperture Radar Observations", *Journal of Geophysical Research*, vol. 91, no. B5, pg. 4993-4999, April 10, 1986.

[5] Massonnet, D. and K. L. Feigl, "Discrimination of Geophysical Phenomena In Satellite Radar Interferograms", *Geophysical Research Letters*, vol. 22, no. 12, pg. 1537-1540, June 15, 1995.

[6] Schwäbisch, M., M. Matschke, W. Knöpfle, and A. Roth, "Quality Assessment of INSAR-Derived DEMs Generated With ERS Tandem Data", *Proceedings of IGARSS'96*, pg. 802-804, 1996.

[7] Kenyi, L. W. and Hannes Raggam, "Atmospheric Induced Errors In Interferometric DEM Generation", *Proceedings of IGARSS'96*, pg. 353-355, 1996.

FIGURES

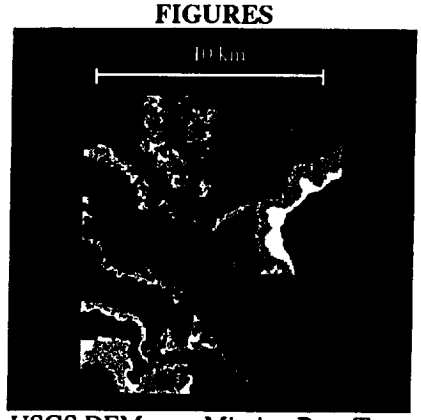

Fig. 1: USGS DEM over Mission Bay, Texas, USA

Fig. 2: TOPSAR DEM over Mission Bay, Texas, USA

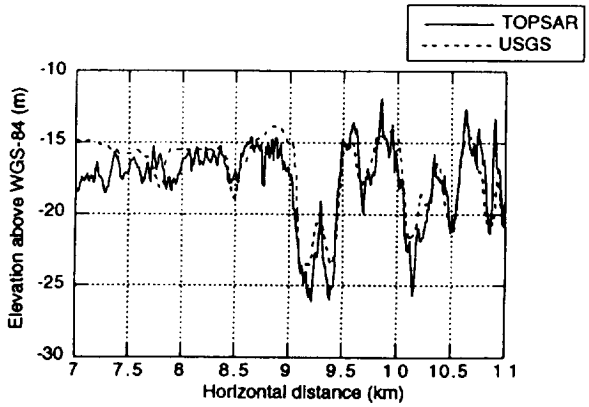

Fig. 3: Transects extracted from co-registered DEMs

Appendix B

Manuscript submitted to the 1997 International Geoscience and Remote Sensing Symposium to be held August 4 to 8 in Singapore.

Multisensor Classification of Wetland Environments Using Airborne Multispectral and SAR Data

Michael R. Ricard[1], Amy L. Neuenschwander[1], Melba M. Crawford[1], and James C. Gibeaut[2]
[1]Center for Space Research, University of Texas at Austin, 3925 W. Braker Ln., Suite 200, Austin, TX 78759-5321
[2]Bureau of Economic Geology, University of Texas at Austin, Campus Mail Code: E0630, Austin, TX 78712
Ph: (512) 471-5573 Fax: (512) 471-3570 E-mail: ricard@csr.utexas.edu

Abstract - Near concurrent airborne data were acquired over the wetlands of the Bolivar Peninsula on the Texas coast by the NASA/JPL AIRSAR (June 28, 1996) and NASA/Stennis Space Center Calibrated Airborne Multispectral Scanner (CAMS) (July 3, 1996), both at 4m spatial resolution. Several approaches which utilize information from both sensors are investigated for classifying the landcover in these data sets. Differences in statistical characteristics of the data necessitate individual parametric models for observations from each sensor, so data are initially classified separately, then a final classification is obtained by combining results from the statistical models using different multisensor integration techniques. These integrated results are compared to single-sensor classification results, as well as to a multisensor classification based on artificial neural networks.

INTRODUCTION

The primary objective of classification of remotely sensed data is often to map landcover. Because different information is provided by various sensors, it can be advantageous to jointly utilize the information of the multisensor data in the classification process. In order to optimally exploit this potentially expanded information set in the classification framework, issues of sensor characteristics, differences in time of acquisition, and target/sensor dependent information content must be addressed.

Over the past several years, a significant amount of research has focused on multisource and/or multisensor classification for remote sensing applications. In [1] and [2], the authors classify multisource data consisting of digital imagery (Landsat MSS) and ancillary information (elevation, slope, and aspect data). Since these data cannot be represented by a single multivariate statistical model, the authors utilize consensus theoretic methods to combine the results of single-source statistical classifiers. In [3], the authors classify multisensor data (optical and SAR) using structured classifiers based on artificial neural networks, thus avoiding the need for modeling the statistical distribution of the data and treating each source or sensor separately.

Based on these issues, there were three objectives of this study. The first was to classify the landcover present in a wetland environment using remotely sensed data from several sensors. Part of this process involved assessing the accuracy of single-sensor classification, as well as determining the advantages and potential problems associated with the use of data from each sensor. By performing multisensor integration of single-sensor classifier outputs, it could be determined whether an improved classification was achieved, as well as whether sensor integration enabled the detection of "hard" classes, i.e. those classes which had lower probabilities of correct classification for a given sensor. The final objective was to determine, based on the data and single-sensor classifier architecture adopted, how to best integrate the multisensor data for classification of the study area.

The following sections contain descriptions of the test site, the multisensor data acquired for the project, and the methodology used to combine the information from these data sets for the purpose of multisensor classification, as well as preliminary results from analysis of the imagery.

STUDY SITE

Bolivar Peninsula is part of the low relief barrier islands of the Texas coast located at the mouth of Galveston Bay. The test site chosen for this study consists of a salt marsh located at a washover fan on southern Bolivar Peninsula.

For classification purposes, this salt marsh study area is characterized in terms of sub-environments defined by wetland maps [4]. The various landcover types present in these environments include low proximal marsh, high proximal marsh, high distal marsh, and spoil/barren flats, as well as areas consisting of water and trees. The low proximal marsh corresponds to tidal flats comprised of *spartina alterniflora* which experience frequent flooding. High proximal marsh is defined as more continuos areas of *spartina alterniflora* and *salicornia virginica* and are less frequently flooded. High distal marsh is comprised of *spartina patens, salicornia virginica, juncus roemerianus* and lies adjacent to barren sand flats. This area is flooded less frequently than proximal marshes.

MULTISENSOR DATA DESCRIPTION

Two near concurrent airborne data sets were acquired over the study site for the purpose of mapping wetland vegetation. Both 20 MHz and 40 MHz AIRSAR data were acquired by NASA/JPL on June 28, 1996 with a ground resolution of approximately 8m and 4m respectively. Additionally, Calibrated Airborne Multispectral Scanner (CAMS) was flown by NASA/Stennis Space Center on July 3, 1996 with

This work was supported in part by the NASA Topography and Surface Change Program (Grant NAG5-2954) and by the NASA National Space Grant Consortium (Grant NGT40003).

approximately 4m spatial resolution. The CAMS data and the 40 MHz AIRSAR data were selected for multisensor classification due to their common coverage and comparable spatial resolution. The multisensor classification system analyzed data from three sensors: optical, thermal, and radar. The "optical sensor" consisted of the six Landsat bands of the CAMS instrument (Blue-NIR) plus a vegetation index, the thermal sensor recorded the ninth band of the CAMS data, and the NASA AIRSAR system acquired two frequency bands (C,L) of fully polarimetric radar data (six channels total).

CLASSIFICATION METHODOLOGY

An ensemble based approach was adopted for classification of the test site data. Data from each sensor were classified separately, then single-sensor classifier outputs were combined at the sensor integration stage.

Pre-Processing

During the pre-processing phase, radiometric and geometric corrections were applied to the data sets. The CAMS Optical data were corrected for bi-directional reflectance The CAMS Thermal data were empirically corrected for radiometric curvature present as a function of scan angle. The AIRSAR data was passed through a 5x5 enhanced Lee filter to reduce the effects of speckle in the imagery. Geometrically, the AIRSAR data was slant-to-ground range corrected. To enable multisensor classification, the three sensor data sets were co-registered. Finally, each sensor band was normalized to zero mean and standard deviation one for input to the classifiers.

Single-Sensor Classifier

For each sensor, the modular classifier architecture employs an expert classifier trained for each output class. The modularized class-specific expert classifiers are chosen to increase the rate of correct classification since the sensor classifier is not trained to solve the whole problem, just to identify a particular class from all the remainder [5].

A separate radial basis function (RBF) network, based on a mixture of Gaussians distribution for each sensor's class, is used to obtain an estimate of the posterior probability for each class

$$P(C_k|\mathbf{x}) = \sum_{j=1}^{M} w_{kj}\phi_j(\mathbf{x}) \qquad (1)$$

where $\phi_i(\mathbf{x})$ are the local basis functions, w_{kj} are the weights of the network, and M is the number of basis functions [6]. These class distributions are modeled as local kernel functions, in this case as mixtures of Gaussians. Based on this framework, each class-specific RBF network was trained to provide estimates of the posteriors using Moody-Darken three-phase learning.

Sensor Integration

Sensor integration techniques are investigated as ensemble approaches to combining classifiers with the goal to incorporate information from each sensor and thereby increase the performance over that achieved by single-sensor classifiers [5]. Since the classifiers utilized for this study provide estimates of the posterior probabilities for each class, information can be combined via either the sum rule or the product rule [1,7]. The sum rule, or weighted average, is based on a weighted sum of the posterior probabilities of a class for each sensor, whereas the product rule is based on a weighted product of the posterior probabilities of a class for each sensor. The weights can either be chosen to be equal for each sensor, in which case just a simple average of the posteriors is performed, or they can be chosen to represent, for instance, the reliability of a given sensor [1]. A further extension would be to weight the posteriors by the sensor's reliability for a given class, not just its overall reliability.

The final technique employed for sensor integration utilizes an artificial neural network, here an RBF network, trained on the outputs of the single-sensor classifiers.

Multisensor Classifier

For comparison to ensemble based sensor integration techniques, a multisensor classifier was tested to determine if information was lost through the single-sensor classification process. Since the data from each sensor were modeled using a mixture of Gaussians model, a classifier using an expert RBF network for each class was again used to classify the multisensor data jointly from a single input vector.

RESULTS

Single-sensor classifiers based on RBF networks and multisensor integrated classifiers based on ensemble approaches to combining classifiers were used for the classification of the CAMS Optical, CAMS Thermal, and AIRSAR data sets. These results are shown in Table 1.

Single-Sensor Classification

Each single-sensor classifier was trained, validated, and tested on separate data sets consisting of 267 ground truth points collected from each of the six classes: water (1), low proximal marsh (2), high proximal marsh (3), high distal marsh (4), spoil/barren flats (5), and trees (6).

The CAMS Optical data and AIRSAR data were both trained using expert RBFs with a total of 50 basis functions for each, while the CAMS Thermal data were trained using expert RBFs with a total of 40 basis functions for each.

Overall, CAMS Optical performed the best of three sensors, with the only difficulty coming in misclassifying 8% of the low proximal marsh as water. Given the amount of water in the low marshes, this is not surprising.

AIRSAR classified water and trees reasonably well, but had trouble separating both the high proximal marsh from the high distal marsh, as well as, separating the spoil/barren flats from the three marsh types. The similar moisture content and vegetation geometry in the high proximal marsh and high distal marshes are likely the cause of this result.

The CAMS Thermal sensor had trouble separating water and high proximal marsh, separating low proximal marsh and high distal marsh, and performed poorly for trees.

Multisensor Integration Results

A simple average and simple product of the single-sensor classifier results were computed with equal weights for each sensor, 95.2% and 94.9% overall classification rate respectively. Both performed better than the best single-sensor classifier, CAMS Optical, indicating the potential increase in performance through combining classifiers for different sensors, even with naive rules.

A weighted average and weighted product were then computed, with the weights for each sensor based on reliability factors obtained from the validation set's overall classification accuracy for each sensor. These sensor weighted results showed improvement over their equally weighted counterparts, thereby giving credence to influencing the sensor integration process based upon the reliability of a given sensor. Weights based on the reliability of a sensor for a given class were also chosen from the sensor validation set's probability of correct classification for that class. There was no significant improvement in results.

Another sensor integration technique involved using a single RBF network with 100 basis functions trained on the outputs of the single-sensor classifiers. These results were comparable overall to both sensor weighted results.

The final multisensor classification results were obtained from combining the single-sensor data prior to classification and then using them as inputs to the class-specific expert RBF classifiers. The results from this method were the best overall at 96.0%. This is because no information was lost from each of the sensors by classifying them separately.

By utilizing the multisensor data, noticeable improvements were made in the classification accuracy for high proximal marsh, high distal marsh, and trees. This is due to the added information AIRSAR and CAMS Thermal data provide about these classes when used in conjunction with CAMS Optical.

Table 1. Classification Accuracy for Test Sets

	Probability of Correct Classification Class						
Classifier	1	2	3	4	5	6	Overall
CAMS Optical	97.4	86.5	95.9	89.5	97.8	92.1	93.2
AIRSAR	94.0	72.7	68.9	72.3	53.9	82.0	74.1
CAMS Thermal	61.8	33.0	50.2	67.0	77.2	39.7	54.8
Sensor Wgt. Average	98.9	92.1	94.8	93.6	97.8	97.4	95.8
Sensor Wgt. Product	98.9	93.6	94.8	93.3	97.0	97.8	95.8
RBF Network	96.6	93.6	94.8	91.8	98.5	99.3	95.8
Joint Classifier	98.9	92.5	95.9	93.6	97.0	98.7	96.0

CONCLUSIONS

Remotely sensed data from multiple sensors were classified both on a single-sensor and multisensor basis. Of the single-sensor classifiers, the CAMS Optical performed the best for each individual class and overall. When multisensor integration was performed on single-sensor classifiers, increases in classification rates were obtained for all techniques when compared to the best single-sensor classifier, CAMS Optical. This highlights the fact that additional information can be gained by combining the results from the classification of individual sensors.

Comparing the multisensor integration techniques, sensor weighted sum and product rules performed better than their equally weighted versions, demonstrating the need for utilizing sensor reliability measures into the classification scheme. Of these sensor integrated results, in addition to the RBF network integrator, all produced comparable results.

The best overall classification rate was obtained from the joint classification of the three sensors using an RBF network based on a mixture of Gaussians distribution for each class. While the percent increase was not sizable, it shows that some information was lost in classifying each sensor separately; that by combining the three sensors into a single classifier input vector, the CAMS Thermal and AIRSAR were able to provide useful information to the classification of the CAMS Optical data set. However, in general, flexibility is lost in classification of a combined data set in terms of the potential use of statistical classification techniques in conjunction with fusion of results via neural networks.

REFERENCES

[1] J.A. Benediktsson and P.H. Swain, "Consensus Theoretic Classification Methods", *IEEE Transactions on Systems Man and Cybernetics*, vol. 22, no. 4, pp. 688-704, July/August 1992.

[2] J.A. Benediktsson, J.R. Sveinsson, and P.H. Swain, "Hybrid Consensus Theoretic Classification", In *Proceedings of International Geoscience and Remote Sensing Symposium*, vol. III, pp. 1848-1850, 1996.

[3] S.B. Serpico and F. Roli, "Classification of Multisensor Remote-Sensing Images by Structured Neural Networks", *IEEE Transactions on Geoscience and Remote Sensing*, vol. 33, no. 3, pp. 562-578, May 1995.

[4] W.A. White, T.R. Calnan, R.A. Morton, R.S. Kimble, T.G. Littleton, J.H. McGowen, H.S. Nance, and K.E. Schmedes, *Submerged Lands of Texas, Galveston-Houston Area*, Bureau of Economic Geology, University of Texas at Austin, 1985.

[5] A.J.C. Sharkey, "On Combining Artificial Neural Nets", *Connection Science*, 8(3/4), 1996.

[6] C.M. Bishop, *Neural Networks for Pattern Recognition*, Oxford: Clarendon Press, 1995.

[7] J. Kittler, M. Hatef, and R.P.W. Duin, "Combining Classifiers", In *Proceedings of International Conference on Pattern Recognition*, vol. II, pp. 897-901, 1996.

Appendix C

Abstract of poster submitted at the Fourth International Conference, Remote Sensing for Marine and Coastal Environments held March 17-19, 1997 in Orlando, Florida.

MAPPING BARRIER ISLANDS USING AIRSAR

(Topic addressed: mapping and charting, acoustic/lidar/SAR or coastal hazards, beach erosion or flooding.

James C. Gibeaut,* K. Clint Slatton,** Melba M. Crawford,** and Roberto Gutierrez*

*Bureau of Economic Geology
The University of Texas at Austin
Austin, Texas 78713-8924
(gibeautj@begv.beg.utexas.edu)

**Center for Space Research
The University of Texas at Austin
Austin, Texas 78759-5321
(crawford@csr.utexas.edu)

The Bureau of Economic Geology and the Center for Space Research at the University of Texas at Austin are developing techniques and determining the capability of airborne synthetic aperture radar (SAR) to map sedimentary environments and geomorphic features on sandy barrier islands. Fully polarimetric multiband (C, L, and P) SAR and C- and L-band topographic SAR data collected by the NASA/JPL airborne system are being analyzed in conjunction with ground measurements and surveys. The study area is along the southeast Texas coast and consists of washover fan/flood-tidal delta complexes, marshes, tidal creeks, beach ridges, vegetated barrier flats, foredunes, and beaches. Responses in the radar data corresponding to variations in vegetation, sediment type, and moisture content are visually apparent and allow the mapping of these features.

L-band (24 cm wavelength) appears to best delineate beach ridge and swale morphology and different wetland environments. L- and P-band (68 cm wavelength) appear to indicate extensions of tidal creeks and faults cutting across the islands. L- and P-band can also delineate former breaches caused by storms and dredging. C-band (5.7 cm wavelength) provides the greatest detail related to vegetation. Radar data also detected subtidal features, wave refraction, and current patterns in a shallow tidal inlet systems.

Appendix D

Abstract of Master of Science in Engineering Thesis by Clint Slatton.

Slatton, K. C., 1997, Simulating synthetic aperture radar backscatter from wetland environments. unpublished masters thesis, College of Engineering, The University of Texas at Austin, 151 p.

Abstract

Simulating Synthetic Aperture Radar Backscatter from Wetland Environments

Kenneth Clinton Slatton, M. S. E.

The University of Texas at Austin, 1997

Supervisor: Byron D. Tapley

A numerical model is developed to simulate the Synthetic Aperture Radar (SAR) scattering from a coastal wetland environment. The simulation is matched to measured scattering data to investigate the utility of relating simulated and actual SAR data for terrain analysis. The model is able to accurately simulate most wetland environments, and it demonstrates that simulating SAR returns is an extremely useful technique for understanding observed scattering behavior.

In the simulation, vegetation-covered terrain is represented as a discrete random-media layer over a rough surface. A random-media model is adapted and integrated with a random-surface model to calculate the SAR backscattering coefficients. The random-media portion of the model uses the wave approach and the distorted Born approximation to calculate scattering within the vegetation layer. The random-surface portion of the model uses the Kirchhoff scalar approximation method to calculate the scattering from the surface.

The model is applied to a study area on the coast of Texas, USA, which encompasses coastal wetland environments on Galveston Island and Bolivar Peninsula. The wetlands occur on the landward sides of these barrier complexes in characteristic zonation patterns. Fully-polarimetric multi-frequency SAR data were acquired over the study area in April 1995. Four prevalent environments, that are distinguishable in the SAR data, are selected for investigation.

SAR data from the four identified environments are characterized as a function of incidence angle, and the model inputs are specified so that the simulated data match the observed data. The simulated backscattering coefficients and model input parameters are used to determine what scattering mechanisms produce the observed SAR returns. The scattering mechanisms are then attributed to surface and vegetation properties that were observed in the study area.